

ADMM-Q: An Improved Hessian-based Weight Quantizer for Post-Training Quantization of Large Language Models

Ryan Lucas* Mehdi Makni* Xiang Meng* Adam Deng
MIT Operations Research Center

Rahul Mazumder
MIT Sloan School of Management
MIT Operations Research Center
MIT Center for Statistics

*Equal contribution

Abstract

Quantization is an effective strategy to reduce the storage and computation footprint of large language models (LLMs). Post-training quantization (PTQ) is a leading approach for compressing LLMs. Popular weight quantization procedures, including GPTQ and RTN, suffer in model utility, especially at aggressive quantization levels (sub-4-bit). We propose ADMM-Q, a novel weight quantization algorithm that considers the layer-wise quantization problem. Our algorithm is based on a combinatorial variant of the Alternating Direction Method of Multipliers (ADMM). Our operator-splitting procedure updates weights continuously to minimize the layer-wise reconstruction error, while gradually enforcing the quantization constraints with convergence guarantees. We propose additional algorithmic enhancements (e.g., penalty scheduling, preconditioning, and a local search post-processing step) to make ADMM-Q efficient at LLM scale. ADMM-Q is modular and can be used as a drop-in replacement for any weight quantizer within existing quantization pipelines: ADMM-Q is fully composable with existing techniques including range clipping, learned or random rotations, and activation scaling. Using ADMM-Q in place of GPTQ on Qwen3-8B, we decrease WikiText-2 perplexity in: (i) the W3A16 weight-only setting (12.85 \rightarrow 10.06); (ii) the W4A8 SmoothQuant procedure (9.29 \rightarrow 8.68); and (iii) the W2A4KV4 SpinQuant procedure (66.11 \rightarrow 19.42).

1 Introduction

Large Language Models (LLMs) have demonstrated exceptional performance across diverse tasks including complex reasoning (Xu et al., 2025), text generation (Achiam et al., 2023), mathematical problem-solving (Romera-Paredes et al., 2024), and code synthesis (Roziere et al., 2023). However, state-of-the-art LLMs (Achiam et al., 2023; Dubey et al., 2024; Google, 2023) with billions of parameters face substantial deployment challenges due to their computational and memory requirements. These constraints limit real-time applications and deployment on resource-constrained devices, making model compression essential for increasing LLM accessibility while preserving accuracy.

Quantization (Han et al., 2015; Frantar et al., 2022; Lin et al., 2024) has emerged as a practical compression approach for LLMs, reducing weight precision from 16-bit floating point to 4 or fewer bits with minimal accuracy degradation. Weight-only quantization (e.g., W4A16) compresses model storage and memory bandwidth while keeping activations in full precision; weight-and-activation quantization (e.g., W4A4) additionally quantizes activations for faster matrix multiplications (Xiao et al., 2023; Liu et al., 2025). In practice, most post-training quantization (PTQ) pipelines process the model layer by layer, minimizing the reconstruction error $\|\mathbf{X}\widehat{\mathbf{W}} - \mathbf{X}\mathbf{W}\|_F^2$ between the original and quantized layer outputs on a small calibration set. The two standard weight quantizers used in this step are round-to-nearest (RTN) and GPTQ (Frantar et al., 2022).

RTN independently rounds each weight to its nearest quantization grid point post clipping value selection, ignoring inter-weight dependencies entirely. While computationally efficient, this approach is suboptimal because it fails to account for the structure of the reconstruction error landscape—weights with large Hessian entries receive no special treatment. GPTQ addresses this by incorporating Hessian information, but it

processes weights greedily in a column-by-column fashion: after quantizing each column, the remaining weights are updated to compensate for the incurred error. This sequential procedure is sensitive to processing order and accumulates errors across columns.

We propose **ADMM-Q**, a principled weight quantizer that formulates layer-wise quantization as a constrained optimization problem and solves it via the Alternating Direction Method of Multipliers (ADMM) (Boyd et al., 2011). Unlike GPTQ’s greedy column-wise approach, **ADMM-Q** jointly optimizes all weights simultaneously by alternating between a continuous Hessian-weighted update and a discrete quantization projection. **ADMM-Q** is designed as a *drop-in replacement* for RTN or GPTQ within any existing PTQ pipeline, including weight-only quantization pipelines or those that employ rotation-based (Liu et al., 2025) or scaling-based (Xiao et al., 2023; Lin et al., 2024) transformations in addition to learned clipping heuristics (e.g., MSE clipping) for weight-and-activation quantization. Quantization to low bit-widths poses a fundamentally hard discrete optimization problem, and as our experiments demonstrate, the choice of solver has a substantial impact on the resulting model utility-compression trade-off.

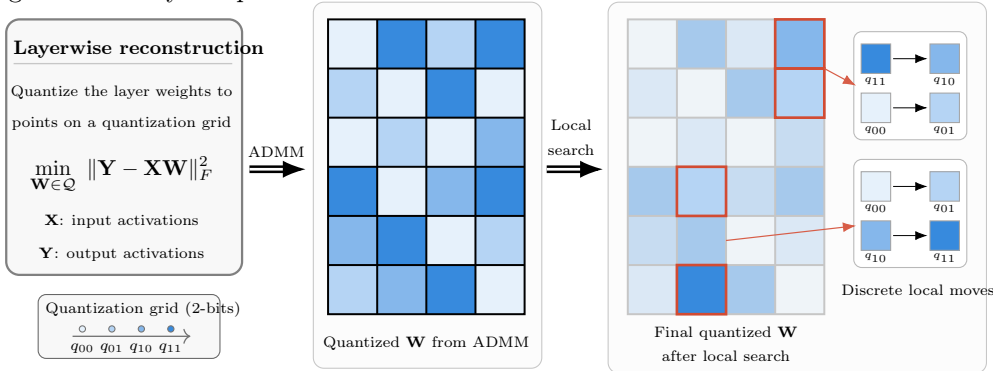


Figure 1: Overview of the proposed **ADMM-Q** algorithm. (Left) The layerwise quantization problem with a reconstruction objective; the goal is to approximate the full-precision weight matrix \mathbf{W} using quantized weights (Section 3). (Middle) ADMM with diagonal scaling and ρ -update scheme (Algorithm 1) to obtain a high-quality quantized weight matrix (Section 3.3). (Right) Starting from the ADMM solution, a local search procedure is applied to further improve the quantized weights and reduce the reconstruction error (Section 3.5).

Our contributions can be summarized as follows:

- We formulate layer-wise weight quantization as a Hessian-weighted constrained optimization problem and propose **ADMM-Q**, an ADMM-based solver with diagonal scaling for numerical stability, an adaptive penalty schedule, and a local-search refinement step for improved discrete solutions. Further, we extend the convergence proof of ADMM established under pruning constraints (Meng et al., 2024) to our setting involving quantization constraints (Theorem 1).
- In weight-only quantization, **ADMM-Q** consistently improves over GPTQ across the Qwen3 model family in perplexity and zero-shot accuracy, with especially large gains in aggressive low-bit regimes such as W3 (Table 1).
- When integrated into existing weight-and-activation quantization pipelines such as SpinQuant and SmoothQuant, **ADMM-Q** continues to improve over GPTQ (Tables 2 and 3). Moreover, when deployed in vLLM it preserves identical inference throughput and memory benefits as GPTQ (for instance, $\approx 1.5x$ speedup at W8A8 on Qwen-32B; Table 4).

2 Related Work

Weight-only quantizers of LLMs. PTQ compresses pre-trained models without retraining by reducing weight and/or activation precision. While activations are quantized on-the-fly during inference, weights are fixed during deployment and can be compressed offline using a specialized optimization procedure. A popular weight quantizer is GPTQ (Frantar et al., 2022), which extends the optimal brain compression

framework (Frantar and Alistarh, 2022; Hassibi and Stork, 1992) to LLM scale by processing weights column by column with Hessian-based error compensation. AWQ (Lin et al., 2024) identifies salient weight channels via activation magnitudes and applies per-channel scaling before RTN. ADMM-Q builds on top of the data-aware layer-wise quantization approach. However, it differs from prior methods by using a joint optimization procedure ADMM as opposed to greedy column-by-column quantization for GPTQ and data-free methods like RTN.

Rotation and scaling transformations. Empirically LLM activations have a high presence of outliers (Xiao et al., 2023), which makes them difficult to quantize online. Several methods reduce quantization difficulty through equivalent model transformations applied before the weight quantizer. SmoothQuant (Xiao et al., 2023) migrates quantization difficulty from activations to weights via per-channel scaling. QuaRot (Ashkboos et al., 2024) applies random Hadamard rotations to reduce the effect of outliers in the quantized network, while SpinQuant (Liu et al., 2025) learns the rotations, followed by RTN or GPTQ weight quantization. These transformation methods are orthogonal to the choice of weight quantizer; in our experiments, we demonstrate that replacing RTN or GPTQ with ADMM-Q gives consistent improvements (4).

ADMM for LLM compression. Prior work has identified that designing joint optimization approaches under model compression constraints can outperform more heuristic methods. Under sparsity constraints, ADMM (Boyd et al., 2011; Davis and Yin, 2016) has been exceptionally successful, outperforming prior heuristic methods such as SparseGPT (Frantar and Alistarh, 2023) and Wanda (Sun et al., 2024). For pure sparsity, Boža (2024) employs ADMM to recover optimal weights on a fixed sparsity support, while Meng et al. (2024) use ADMM for both support identification and weight optimization. Further, Makni et al. (2025) use ADMM to sparse-plus-low-rank decomposition. However, ADMM under quantization remains largely unexplored due to the scale of LLMs and the hard combinatorial structure of the optimization constraints.

3 ADMM-Q

3.1 Problem formulation

As in GPTQ (Frantar et al., 2022) and AWQ (Lin et al., 2024), we compress the model layer by layer, minimizing the reconstruction error between the outputs of the pre-trained weights and the quantized weights on calibration data. For a given layer with pre-trained weight matrix $\widehat{\mathbf{W}} \in \mathbb{R}^{n \times p}$ (n and p correspond to input and output channels, respectively) and input activations $\mathbf{X} \in \mathbb{R}^{N \times n}$ collected from N calibration samples, we solve:

$$\min_{\mathbf{W}} \frac{1}{2} \|\mathbf{X}\widehat{\mathbf{W}} - \mathbf{X}\mathbf{W}\|_F^2 + \frac{\lambda}{2} \|\widehat{\mathbf{W}} - \mathbf{W}\|_F^2 \quad \text{s.t.} \quad \mathbf{W} \in \mathcal{Q} \quad (1)$$

where \mathcal{Q} denotes the set of quantized weight matrices (e.g., 4-bit integers with per-channel scale and zero-point) and $\lambda > 0$ is a regularization parameter. Defining the Hessian $\mathbf{H} = \mathbf{X}^\top \mathbf{X} + \lambda \mathbf{I}$, this is equivalent to:

$$\min_{\mathbf{W}} \frac{1}{2} \text{Tr} \left((\mathbf{W} - \widehat{\mathbf{W}})^\top \mathbf{H} (\mathbf{W} - \widehat{\mathbf{W}}) \right) \quad \text{s.t.} \quad \mathbf{W} \in \mathcal{Q} \quad (2)$$

where $\text{Tr}(\cdot)$ denotes the trace of a matrix. This formulation captures the key challenge: finding quantized weights $\mathbf{W} \in \mathcal{Q}$ that minimize the Hessian-weighted distance to the pre-trained weights. Both RTN and GPTQ can be viewed as approximate solvers for this problem; RTN ignores \mathbf{H} entirely (treating it as the identity), while GPTQ applies a greedy column-wise solver based on the optimal brain compression framework (Hassibi and Stork, 1992; Frantar and Alistarh, 2022). ADMM is natural because it separates the smooth Hessian-weighted objective (continuous weight updates) from the discrete quantization constraint (enforcing the constraints gradually).

3.2 Diagonal scaling for numerical stability

In practice, the activation norms $\|\mathbf{X}_{:,i}\|_2$ vary significantly across input dimensions, leading to a poorly conditioned Hessian \mathbf{H} and unstable optimization. This issue is particularly severe in LLMs, where a small fraction of channels carry disproportionately large activation magnitudes, which is the well-documented

“channel outlier” phenomenon (Xiao et al., 2023; Dettmers et al., 2023). GPTQ sidesteps this issue in part because its greedy procedure conditions on a single diagonal entry of the inverse Hessian at a time, so the condition number is less directly harmful. By contrast, ADMM-Q jointly updates all weights simultaneously through a closed-form solution involving the full Hessian, making it directly sensitive to the condition number of \mathbf{H} . Without preconditioning, outlier channels with large Hessian entries dominate the update, causing slow convergence and numerical instability. We introduce a diagonal scaling that addresses this. Let $\mathbf{\Sigma} = \text{Diag}(\mathbf{H})^{-1/2}$ and define the scaled variable $\mathbf{W}' = \mathbf{\Sigma}^{-1}\mathbf{W}$. Problem (2) becomes:

$$\min_{\mathbf{W}'} \frac{1}{2} \text{Tr} \left((\mathbf{W}' - \mathbf{\Sigma}^{-1}\widehat{\mathbf{W}})^\top \underbrace{(\mathbf{\Sigma}^\top \mathbf{H} \mathbf{\Sigma})}_{\text{scaled Hessian}} (\mathbf{W}' - \mathbf{\Sigma}^{-1}\widehat{\mathbf{W}}) \right) \quad \text{s.t.} \quad \mathbf{\Sigma} \mathbf{W}' \in \mathcal{Q} \quad (3)$$

The scaled Hessian $\mathbf{\Sigma}^\top \mathbf{H} \mathbf{\Sigma}$ has unit diagonal entries, which substantially reduces its condition number. This ensures all channels contribute comparably to the ADMM updates. For notational simplicity, we use \mathbf{W} , $\widehat{\mathbf{W}}$, and \mathbf{H} to denote the scaled quantities, writing:

$$\min_{\mathbf{W}} \frac{1}{2} \text{Tr} \left((\mathbf{W} - \widehat{\mathbf{W}})^\top \mathbf{H} (\mathbf{W} - \widehat{\mathbf{W}}) \right) \quad \text{s.t.} \quad \mathbf{\Sigma} \mathbf{W} \in \mathcal{Q} \quad (4)$$

In our ablation study (Table 6), we find that diagonal preconditioning is one of the most impactful components of ADMM-Q: removing it at W3A16 on Qwen3-8B increases WikiText-2 perplexity from 10.06 to 14.68, worse than the 12.85 of GPTQ.

3.3 ADMM algorithm

To solve the non-convex problem (4), we employ ADMM. We introduce an auxiliary variable \mathbf{D} to decouple the continuous optimization from the quantization constraint:

$$\min_{\mathbf{W}, \mathbf{D}} \frac{1}{2} \text{Tr} \left((\mathbf{W} - \widehat{\mathbf{W}})^\top \mathbf{H} (\mathbf{W} - \widehat{\mathbf{W}}) \right) + \mathbb{I}_{\mathcal{Q}}(\mathbf{\Sigma} \mathbf{D}) \quad \text{s.t.} \quad \mathbf{W} = \mathbf{D} \quad (5)$$

where $\mathbb{I}_{\mathcal{Q}}(\cdot)$ is the indicator function for the quantization set. The augmented Lagrangian with dual variable \mathbf{V} and penalty $\rho > 0$ is:

$$L_\rho(\mathbf{W}, \mathbf{D}, \mathbf{V}) = \frac{1}{2} \text{Tr} \left((\mathbf{W} - \widehat{\mathbf{W}})^\top \mathbf{H} (\mathbf{W} - \widehat{\mathbf{W}}) \right) + \mathbb{I}_{\mathcal{Q}}(\mathbf{\Sigma} \mathbf{D}) + \langle \mathbf{V}, \mathbf{W} - \mathbf{D} \rangle + \frac{\rho}{2} \|\mathbf{W} - \mathbf{D}\|_F^2 \quad (6)$$

The ADMM updates at iteration t are:

$$\mathbf{W}^{(t+1)} = (\mathbf{H} + \rho_t \mathbf{I})^{-1} (\mathbf{H} \widehat{\mathbf{W}} + \rho_t \mathbf{D}^{(t)} - \mathbf{V}^{(t)}) \quad (7)$$

$$\mathbf{D}^{(t+1)} = \arg \min_{\mathbf{\Sigma} \mathbf{D} \in \mathcal{Q}} \|\mathbf{D} - (\mathbf{W}^{(t+1)} + \mathbf{V}^{(t)}/\rho_t)\|_F^2 \quad (8)$$

$$\mathbf{V}^{(t+1)} = \mathbf{V}^{(t)} + \rho_t (\mathbf{W}^{(t+1)} - \mathbf{D}^{(t+1)}) \quad (9)$$

Efficient W-update. By pre-computing the eigendecomposition $\mathbf{H} = \mathbf{U} \mathbf{\Lambda} \mathbf{U}^\top$ once, the matrix inverse in (7) can be evaluated as $(\mathbf{H} + \rho_t \mathbf{I})^{-1} = \mathbf{U} (\mathbf{\Lambda} + \rho_t \mathbf{I})^{-1} \mathbf{U}^\top$ for any ρ_t , reducing each iteration to matrix multiplications.

D-update (quantization projection). The closed form solution for the D-update (8) reduces to RTN; it projects onto the quantization grid, accounting for the scaling $\mathbf{\Sigma}$. For a fixed uniform grid, each block/channel/tensor is solved independently. Given a target $\widetilde{\mathbf{W}}^{(t)} = \mathbf{W}^{(t+1)} + \mathbf{V}^{(t)}/\rho_t$, the quantized values are:

$$\mathbf{\Sigma} \mathbf{D} = \Delta \cdot \text{Round} \left(\frac{\mathbf{\Sigma} \widetilde{\mathbf{W}}^{(t)} - z_0}{\Delta} \right) + z_0 \quad (10)$$

where Δ is the quantization scale and z_0 is the zero-point.

Grid refresh. Let $\theta = (\Delta, z_0)$ denote the scale and zero-point determining the quantization grid $\mathcal{Q}(\theta)$, and notice that $\widetilde{\mathbf{W}}^{(t)}$ is the continuous point that is projected in the **D**-update. As in GPTQ, we initialize $\theta^{(0)}$ by RTN on the dense weights, but as ADMM moves the continuous iterate, this fixed grid can become stale for the current target $\widetilde{\mathbf{W}}^{(t)}$.

We therefore equip ADMM-Q with the ability to refit the grid parameters from the current continuous weights and re-project, while adjusting the dual variable to keep the ADMM state consistent. We visualize this effect in Figure 2: the gray projection continues with the old grid after the iterate has moved, while the blue projection shows the refreshed grid better aligned with the current continuous point. This is a key advantage of the ADMM-Q algorithm compared to GPTQ, which is required to the grid fixed during optimization to avoid compromising prior greedy decisions. We give further details on the grid refresh in Appendix B.

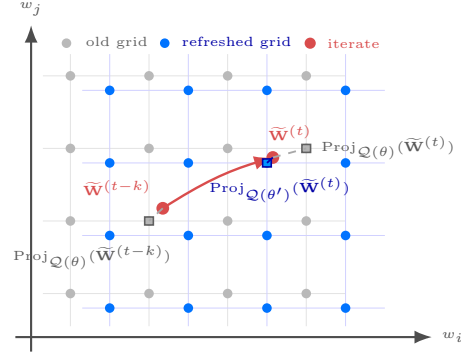


Figure 2: Grid refresh updates the projection to match the current continuous iterate.

3.4 Integration with popular quantization transformations

ADMM-Q modifies only the layer-wise weight quantization step, so it can be inserted into PTQ pipelines. For instance, one can apply equivalent transformations that preserve the layer input-output map, but change the coordinates in which the local reconstruction problem is posed e.g. scaling or rotation; or other techniques such as weight clipping.

- **Scaling** (SmoothQuant (Xiao et al., 2023), AWQ (Lin et al., 2024)): Per-channel scaling can be absorbed into ADMM-Q’s scaling matrix Σ , giving the same layer-wise problem with a modified scaling parameterization.
- **Rotation** (SpinQuant (Liu et al., 2025), QuaRot (Ashkboos et al., 2024)): If rotation matrices are first applied, then ADMM-Q is applied to the corresponding transformed layer-wise reconstruction problem, i.e., the same local quantization objective expressed in the rotated coordinates with the associated Hessian.
- **Clipping Heuristics.** The scale and zero-point in (10) can be set without clipping as follows: $\Delta = (\max - \min)/(2^b - 1)$. Heuristics for learning quantization grid clipping can also be integrated within our framework. In this paper, we employ the default method used in GPTQ and SpinQuant: MSE grid search for clipping ratios using 100 grid points with maximum shrink ratio 0.8 (see Appendix D).

Appendix A gives the form of the modified reconstruction problem for scaling and rotation.

3.5 Local search refinement

Since ADMM updates all weights jointly, the **W**-update may shift many weights in the same direction. Weights near the midpoint of two adjacent grid points are particularly susceptible. This correlated rounding might lead to suboptimal discrete solutions. To reconcile this issue, we propose a highly-efficient *pair-swap* local search as a post-processing step. Once ADMM-Q has converged, the solution \mathbf{W}_q may be improved by discrete local moves that directly reduce the reconstruction error (2).

Setup. Recall $\mathbf{W}_q \in \mathbb{R}^{n \times p}$ (defined in Algorithm 1). Let Δ_j be the per-output-channel scale for column j . Each entry $[\mathbf{W}_q]_{ij}$ takes values on the grid $\{z_j + k \Delta_j : k \in \mathbb{Z}, 0 \leq k \leq 2^b - 1\}$. A *pair-swap* selects two rows i_1, i_2 and, for each column j independently, shifts $[\mathbf{W}_q]_{i_1 j}$ by $\pm \Delta_j$ and $[\mathbf{W}_q]_{i_2 j}$ by $\pm \Delta_j$, subject to staying within the grid bounds.

Algorithm 1: ADMM-Q: ADMM-based Weight Quantization

Require: Pre-trained weights $\widehat{\mathbf{W}}$, Hessian $\mathbf{H} = \mathbf{X}^\top \mathbf{X} + \lambda \mathbf{I}$, bit-width b , iterations T , initial penalty ρ_0 , growth factor $\gamma > 1$

Ensure: Quantized weights \mathbf{W}_q

- 1: $\Sigma \leftarrow \text{Diag}(\mathbf{H})^{-1/2}$ // Scaling matrix
- 2: $\widehat{\mathbf{W}} \leftarrow \Sigma^{-1} \widehat{\mathbf{W}}$, $\mathbf{H} \leftarrow \Sigma^\top \mathbf{H} \Sigma$ // Scale problem
- 3: $\mathbf{U} \mathbf{A} \mathbf{U}^\top \leftarrow \text{eig}(\mathbf{H})$ // Eigendecomposition
- 4: $\mathbf{D}^{(0)} \leftarrow \widehat{\mathbf{W}}$, $\mathbf{V}^{(0)} \leftarrow \mathbf{0}$
- 5: **for** $t = 0, 1, \dots, T - 1$ **do**
- 6: $\mathbf{W}^{(t+1)} \leftarrow \mathbf{U}(\mathbf{I} + \rho_t \mathbf{I})^{-1} \mathbf{U}^\top (\mathbf{H} \widehat{\mathbf{W}} + \rho_t \mathbf{D}^{(t)} - \mathbf{V}^{(t)})$ // W-update
- 7: $\mathbf{D}^{(t+1)} \leftarrow \Sigma^{-1} \text{Proj}_{\mathcal{Q}}(\Sigma(\mathbf{W}^{(t+1)} + \mathbf{V}^{(t)}/\rho_t))$ // Quantize
- 8: $\mathbf{V}^{(t+1)} \leftarrow \mathbf{V}^{(t)} + \rho_t(\mathbf{W}^{(t+1)} - \mathbf{D}^{(t+1)})$ // Dual update
- 9: $\rho_{t+1} \leftarrow \text{update}(\rho_t)$
- 10: **end**
- 11: $\mathbf{W}_q \leftarrow \Sigma \mathbf{D}^{(T)}$
- 12: $\mathbf{W}_q \leftarrow \text{PAIRSWAP}(\mathbf{W}_q, \widehat{\mathbf{W}}, \mathbf{H})$ // Local search (3.5)
- 13: **return** \mathbf{W}_q

Closed-form cost. The reconstruction error (2) decomposes as a sum over output columns: $\mathcal{L} = \sum_{j=1}^p \epsilon_j^\top \mathbf{H} \epsilon_j$, where $\epsilon_j = (\mathbf{W}_q - \widehat{\mathbf{W}})_{:,j} \in \mathbb{R}^n$. Perturbing rows i_1, i_2 in column j by $\delta_{i_1 j}, \delta_{i_2 j} \in \{+\Delta_j, -\Delta_j\}$ changes the loss contribution of column j by

$$\Delta \mathcal{L}_{i_1, i_2, j} = -2 \delta_{i_1 j} G_{i_1 j} + \delta_{i_1 j}^2 H_{i_1 i_1} - 2 \delta_{i_2 j} G_{i_2 j} + \delta_{i_2 j}^2 H_{i_2 i_2} + 2 \delta_{i_1 j} \delta_{i_2 j} H_{i_1 i_2}, \quad (11)$$

where $\mathbf{G} = \mathbf{H}(\widehat{\mathbf{W}} - \mathbf{W}_q)$ is the gradient of the objective. Only three Hessian entries and two gradient entries are needed to evaluate swapping a pair with column j and rows i_1 and i_2 . Evaluating all potential swaps is made extremely efficient through GPU parallelization in our implementation.

Algorithm. For a given row pair (i_1, i_2) , each output column j selects the best sign combination among $\{(\pm \Delta_j, \pm \Delta_j)\}$ via (11). First, we compute \mathbf{G} (one matrix-multiplication cost). Then each round proceeds as follows: (i) sample random row pairs in batches; (ii) evaluate (11) for all four sign combinations per column; (iv) apply the pair with the largest total improvement; (v) update \mathbf{G} via a rank-2 correction: $\mathbf{G} \leftarrow \mathbf{G} - \mathbf{H}_{:, \{i_1, i_2\}} [\delta_{i_1, :}; \delta_{i_2, :}]$, where $\delta_{i, :} \in \mathbb{R}^{1 \times p}$ is the applied perturbation for row i . We run at most 5 rounds. Our ablation studies (Table 7) show that local search is especially impactful on LLaMA models within SpinQuant at W4A4KV4, where removing it increases WikiText-2 perplexity from 7.26 to 7.97 on LLaMA-3 8B and from 15.55 to 19.45 on LLaMA-3.2 1B-Instruct.

3.6 Convergence

Theorem 1. Let $\{\mathbf{D}^{(t)}\}_{t=0}^\infty$ and $\{\mathbf{W}^{(t)}\}_{t=0}^\infty$ be the sequences generated by 1. Suppose the penalty parameters $\{\rho_t\}_{t=1}^\infty$ satisfy $\sum_{t=1}^\infty 1/\rho_t < \infty$. Then for any $t \geq 1$:

$$\max \left\{ \|\mathbf{D}^{(t+1)} - \mathbf{D}^{(t)}\|_F, \|\mathbf{W}^{(t+1)} - \mathbf{D}^{(t+1)}\|_F \right\} \leq \frac{C}{\rho_t} \quad (12)$$

where C is a constant depending on \mathbf{X} , $\widehat{\mathbf{W}}$, λ , and $\sum_{t=1}^\infty 1/\rho_t$. In particular, there exists a quantized matrix $\bar{\mathbf{D}}$ such that $\mathbf{D}^{(t)} \rightarrow \bar{\mathbf{D}}$ and $\mathbf{W}^{(t)} \rightarrow \bar{\mathbf{D}}$ as $t \rightarrow \infty$.

The condition $\sum 1/\rho_t < \infty$ is satisfied by, e.g., $\rho_t = \rho_0 \cdot \gamma^t$ with $\gamma > 1$, which is the schedule used in Algorithm 1. This guarantees that the continuous and discrete iterates converge to the same limit point, ensuring the constraint $\mathbf{W} = \mathbf{D}$ is asymptotically satisfied. Theorem 1 extends the convergence guarantee of ADMM in the sparsity setting (Meng et al., 2024) to quantization, including under grid refresh. The proof is deferred to Appendix C.

4 Experimental results

4.1 Experimental setup

Models and evaluation protocol. We evaluate ADMM-Q across three settings: (i) weight-only quantization on the Qwen3 model family (1.7B, 4B, 8B, 14B, 32B); (ii) weight-and-activation quantization with SpinQuant (Liu et al., 2025) on LLaMA-3 8B (Dubey et al., 2024), LLaMA-3.2 1B-Instruct, and Qwen3-8B; and (iii) weight-and-activation quantization with SmoothQuant (Xiao et al., 2023) on Qwen3-8B. We report perplexity (\downarrow) on WikiText-2, C4, and Penn Treebank (PTB), and zero-shot accuracy (\uparrow) averaged over nine tasks. For zero-shot evaluation, we use the LM Evaluation Harness (Gao et al., 2023) on PIQA (Bisk et al., 2020), ARC-Easy/Challenge (Clark et al., 2018), HellaSwag (Zellers et al., 2019), Winogrande (Sakaguchi et al., 2021), RTE (Poliak, 2020), OpenbookQA (Banerjee et al., 2019), BoolQ (Clark et al., 2019), and Social IQa (Sap et al., 2019).

4.2 Numerical results

Weight-only quantization on the Qwen3 model family. Table 1 compares GPTQ, AWQ and ADMM-Q under weight-only W4/3/2 per-channel quantization across five Qwen3 model sizes (1.7B–32B). ADMM-Q consistently improves over GPTQ on WikiText-2, C4, and PTB perplexity across bit-widths, with larger gains at W3 and W2 where the quantization problem is more challenging. For example, on Qwen3-8B at W3, ADMM-Q reduces WikiText-2 perplexity from 12.85 to 10.06 and PTB perplexity from 35.01 to 27.30. Zero-shot accuracy follows a similar trend. AWQ is strong at W4 but less competitive at W3 and W2, perhaps because it uses RTN as its weight quantizer. To understand the source of improvements, Figure 3 compares the layer-wise reconstruction error of ADMM-Q relative to GPTQ on Qwen3-8B under W4 and W3 per-channel quantization. ADMM-Q achieves lower reconstruction error across all 36 decoder layers, with largest relative gains in early layers, where ADMM-Q reduces reconstruction error to as low as 10% of GPTQ’s. In later layers, ADMM-Q consistently retains roughly 70–75% of GPTQ’s error, both at W3 and W4. In Appendix D, Table 5 we report wall-clock quantization time and peak GPU memory usage for GPTQ and ADMM-Q across all Qwen3 models. The runtime grows with model size, but remains practical: even at 32B, quantization completes in under two hours on a single GPU. We also measure peak GPU memory during quantization; GPTQ is 6% less memory-intensive. Since weight quantization is a one-time step, we view the modest increase in runtime and memory as acceptable tradeoffs for the consistent gains in perplexity and zero-shot accuracy.

Weight-and-activation quantization with SpinQuant and SmoothQuant. We evaluate ADMM-Q as a drop-in replacement for GPTQ within the SpinQuant (Liu et al., 2025) pipeline on Qwen3-8B, LLaMA-3 8B, and LLaMA-3.2 1B-Instruct and the SmoothQuant (Xiao et al., 2023) pipeline on Qwen3-8B. SpinQuant applies learned rotation matrices (R_1, R_2) to the model weights before quantization, and optionally uses online Hadamard transforms (R_3, R_4) for activation and KV cache quantization. We compare GPTQ and ADMM-Q across three weight bit-widths (2, 3, 4) with 4-bit activation and KV cache quantization (WbA4KV4), using four weight quantizer settings: symmetric/asymmetric \times per-channel/groupsizes-128. For GPTQ and ADMMQ we use the default configuration for rotation optimization W16A4KV4 rotation optimization for (WbA4KV4) quantization. For RTN, we use a single rotation optimized at W4A4KV4. Results are reported in Tables 2 and 3.

Model	Wiki-2 PPL (\downarrow)				C4 PPL (\downarrow)				PTB PPL (\downarrow)				0-shot Acc. (\uparrow)			
	Dense	GPTQ	AWQ	ADMM-Q	Dense	GPTQ	AWQ	ADMM-Q	Dense	GPTQ	AWQ	ADMM-Q	Dense	GPTQ	AWQ	ADMM-Q
W4																
1.7B-Base	9.40	12.40	11.08	11.24	15.42	20.88	17.53	18.94	25.37	37.58	30.10	32.51	62.54	56.58	60.19	58.34
4B-Base	7.90	8.58	9.20	8.55	13.31	14.60	14.87	14.57	19.68	22.08	22.67	22.12	66.72	64.96	65.03	65.63
8B-Base	7.00	7.82	8.06	7.56	11.91	13.39	13.14	13.01	17.12	19.82	19.26	19.04	69.07	68.93	67.95	68.14
14B-Base	6.38	6.87	7.28	6.79	10.99	11.91	12.05	11.83	15.30	16.81	16.99	16.54	71.75	70.76	69.82	71.07
32B	7.61	8.22	8.44	8.06	12.45	13.58	13.54	13.55	18.82	20.84	21.18	20.79	71.49	69.98	69.68	69.14
W3																
1.7B-Base	9.40	24.48	34.55	16.39	15.42	50.55	49.96	37.96	25.37	117.14	159.65	52.95	62.54	43.65	46.06	46.78
4B-Base	7.90	13.64	21.30	12.85	13.31	24.84	28.29	24.49	19.68	41.42	60.86	38.49	66.72	50.89	49.74	52.40
8B-Base	7.00	12.85	17.28	10.06	11.91	21.27	22.93	18.25	17.12	35.01	48.55	27.30	69.07	54.43	51.08	57.80
14B-Base	6.38	9.50	14.34	8.16	10.99	18.03	19.50	15.35	15.30	30.12	39.31	22.14	71.75	64.73	53.45	66.53
32B	7.61	10.70	16.82	9.82	12.45	18.65	23.06	17.76	18.82	32.13	65.32	28.70	71.49	62.92	60.28	65.75
W2																
1.7B-Base	9.40	441.72	2.5e7	42.72	15.42	1301.16	2.7e7	252.47	25.37	1472.54	2.2e7	199.86	62.54	36.74	37.37	37.62
4B-Base	7.90	27.75	1.9e7	24.04	13.31	72.68	2.1e7	66.07	19.68	101.48	2.2e7	91.55	66.72	42.54	36.61	43.01
8B-Base	7.00	32.88	3.4e7	17.69	11.91	89.37	2.8e7	45.31	17.12	145.36	3.1e7	61.68	69.07	41.40	37.86	47.06
14B-Base	6.38	40.98	2.1e7	12.62	10.99	125.90	1.9e7	36.45	15.30	177.38	1.9e7	45.22	71.75	41.67	37.50	51.58
32B	7.61	35.95	5.1e6	18.15	12.45	553.18	4.4e6	50.00	18.82	147.86	3.9e6	66.01	71.49	52.77	36.57	55.65

Table 1: Performance of Qwen3 under 4-bit (W4), 3-bit (W3), and 2-bit (W2) symmetric per-channel weight-only quantization, comparing GPTQ, AWQ, and ADMM-Q. Note: the 32B-Base model is not yet released, so we use <https://huggingface.co/Qwen/Qwen3-32B>.

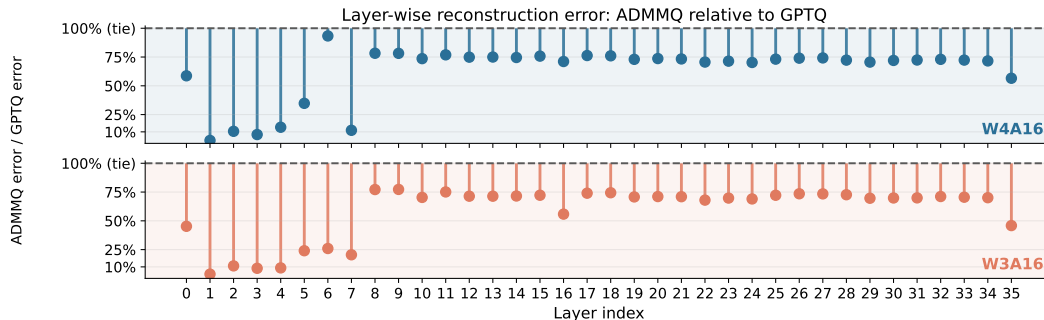


Figure 3: Layer-wise reconstruction error of ADMM-Q relative to GPTQ on Qwen3-8B-Base under W4 (top) and W3 (bottom) per-channel weight-only quantization. Each point shows ADMM-Q error/GPTQ error; values below the 100% line indicate ADMM-Q achieves lower error.

Config	Wt. Quant	Wiki-2 PPL (\downarrow)			C4 PPL (\downarrow)			PTB PPL (\downarrow)			0-shot Acc. (\uparrow)		
		RTN	GPTQ	ADMM-Q	RTN	GPTQ	ADMM-Q	RTN	GPTQ	ADMM-Q	RTN	GPTQ	ADMM-Q
LLaMA-3 8B													
BF16 (dense)		6.14			9.44			14.84			63.94		
W4A4KV4	S, per-ch	7.95	7.34	7.26	13.44	12.16	12.08	19.94	17.94	17.74	58.55	60.55	60.52
	S, g128	8.99	7.27	7.21	14.92	12.07	11.98	22.00	17.75	17.52	56.61	59.02	60.17
	A, per-ch	8.11	7.35	7.24	13.58	12.14	12.05	19.97	17.92	17.66	58.71	59.44	60.26
	A, g128	9.22	7.26	7.17	15.27	11.94	11.86	21.59	17.74	17.45	56.22	59.72	60.86
W3A4KV4	S, per-ch	109.11	8.50	8.02	117.26	15.01	14.29	303.58	21.27	20.13	38.01	56.51	57.59
	S, g128	97.34	8.40	8.01	112.94	14.79	14.11	283.83	20.82	19.86	38.81	56.08	57.29
	A, per-ch	111.04	8.25	8.05	137.82	14.34	14.27	370.68	20.73	20.24	37.69	56.31	57.91
	A, g128	70.16	8.14	7.91	66.87	13.93	13.82	167.00	20.17	19.68	40.85	57.14	58.34
W2A4KV4	S, per-ch	1.6e6	50.27	15.65	1.7e6	179.57	45.33	1.9e6	160.66	74.80	35.47	39.52	45.63
	S, g128	2.0e6	29.36	15.22	1.9e6	89.24	43.63	1.9e6	114.14	58.67	35.48	40.47	44.64
	A, per-ch	5777	16.39	14.95	4214	40.18	42.12	4289	60.55	58.14	34.73	42.70	44.79
	A, g128	6777	15.32	14.02	6030	36.16	35.68	5608	51.00	47.44	34.53	42.44	47.55
LLaMA-3.2 1B-Instruct													
BF16 (dense)		13.16			21.30			37.31			53.22		
W4A4KV4	S, per-ch	15.97	15.81	15.55	27.79	26.11	25.80	53.59	48.69	47.76	47.74	48.27	49.31
	S, g128	19.33	15.67	15.42	31.94	25.76	25.34	62.57	47.55	47.53	46.75	49.01	49.72
	A, per-ch	17.09	15.74	15.60	29.37	25.85	25.69	55.43	48.59	47.18	46.90	48.77	49.38
	A, g128	20.05	15.50	15.26	31.94	25.39	25.36	60.66	47.39	47.35	47.18	48.52	49.36
W3A4KV4	S, per-ch	96.35	19.70	17.88	159.31	34.07	31.16	318.13	65.22	56.65	38.61	45.76	46.84
	S, g128	149.68	19.33	18.06	227.31	33.50	31.26	438.08	61.71	55.99	37.54	45.62	46.70
	A, per-ch	206.10	18.99	18.05	355.45	32.43	31.37	568.98	60.91	57.47	36.99	45.78	46.15
	A, g128	169.17	18.40	17.55	209.44	30.90	30.32	374.47	58.43	56.59	37.14	45.88	47.26
W2A4KV4	S, per-ch	2.5e6	172.16	43.98	2.1e6	382.96	123.33	2.5e6	489.33	157.51	36.67	36.85	39.86
	S, g128	2.8e6	131.90	44.45	2.7e6	370.65	138.69	2.6e6	440.34	184.64	36.94	37.74	38.67
	A, per-ch	1.2e4	46.40	41.84	1.2e4	135.55	123.04	1.1e4	195.94	166.27	34.58	38.20	39.26
	A, g128	1.3e4	46.76	37.95	1.2e4	118.29	95.90	1.6e4	174.98	140.65	36.05	40.05	39.09

Table 2: RTN, GPTQ, and ADMM-Q within the SpinQuant pipeline across two LLaMA models and weight bit-widths 2, 3, 4 (all WbA4KV4). ‘‘S’’ = symmetric, ‘‘A’’ = asymmetric; ‘‘per-ch’’ = per-channel, ‘‘g128’’ = groupsizes 128. Best result per cell is **bolded**.

Config	Wt. Quant	Wiki-2 PPL (\downarrow)		C4 PPL (\downarrow)		PTB PPL (\downarrow)		0-shot Acc. (\uparrow)	
		GPTQ	ADMM-Q	GPTQ	ADMM-Q	GPTQ	ADMM-Q	GPTQ	ADMM-Q
Qwen3-8B (SmoothQuant, WbA8)									
BF16 (dense)		7.00		11.91		17.12		69.08	
W4A8	per-ch	9.29	8.68	16.82	15.69	25.60	23.44	65.74	66.10
W3A8	per-ch	16.00	12.21	31.13	24.98	50.62	38.14	54.91	54.64
W2A8	per-ch	130.04	18.89	204.11	68.70	268.67	79.65	41.38	46.13
Qwen3-8B (SpinQuant, WbA4KV4)									
BF16 (dense)		7.00		11.91		17.12		69.08	
W4A4KV4	per-ch	11.80	11.77	20.84	20.82	37.64	37.58	57.67	57.96
W3A4KV4	per-ch	13.70	13.11	25.57	24.40	43.19	41.35	53.97	54.70
W2A4KV4	per-ch	66.11	19.42	3324.38	59.27	200.41	81.67	43.28	46.29

Table 3: GPTQ vs. ADMM-Q on Qwen3-8B-Base across: weight-and-activation (WbA8), and SpinQuant (WbA4KV4). Best result per cell is **bolded**.

Inference speed-ups in VLLM. We integrate ADMM-Q into the llm-compressor/vLLM stack and benchmark inference latency at W8A8 under both SmoothQuant and SpinQuant on Qwen3 models (8B, 14B, 32B). Table 4 reports speedups relative to the dense BF16 baseline, measured over 2000 Wikitext-2 sequences pro-

cessed in batches of 100. We use 800 tokens of pre-fill and 256 tokens of decoding. Both GPTQ and ADMM-Q achieve nearly identical throughput gains: for example, on Qwen3-32B with SpinQuant W8A8, ADMM-Q achieves a $1.52\times$ speedup, matching GPTQ’s $1.52\times$. This is expected since both methods produce weight matrices in the same quantized format and differ only in the offline optimization procedure used to obtain them. We note that vLLM does not currently support W4A4 inference kernels on standard NVIDIA hardware, though hardware and kernel support for sub-8-bit weight-and-activation quantization is under active development. In Table 5, we also provide inference memory and storage memory for GPTQ and ADMM-Q, and show that they are also close to identical.

Method	8B-Base	14B-Base	32B
Dense BF16	1.0000	1.0000	1.0000
SmoothQuant W8A8			
GPTQ	1.2393 ± 0.0012	1.3722 ± 0.0010	1.4844 ± 0.0023
ADMM-Q	1.2408 ± 0.0012	1.3827 ± 0.0029	1.4808 ± 0.0012
SpinQuant W8A8			
GPTQ	1.2554 ± 0.0014	1.3918 ± 0.0008	1.5158 ± 0.0035
ADMM-Q	1.2507 ± 0.0015	1.3977 ± 0.0041	1.5220 ± 0.0015

Table 4: Inference latency speedup relative to the dense BF16 baseline for Qwen3 models in VLLM under GPTQ and ADMM-Q. Results are computed over 2000 sequences (processed in batches of 100). Values are reported as mean \pm standard error.

5 Conclusion and limitations

We introduce ADMM-Q, a principled layer-wise quantization method for post-training quantization of LLMs based on ADMM. By formulating layer-wise quantization as a Hessian-weighted constrained reconstruction problem, ADMM-Q jointly optimizes the quantized weights within each layer rather than processing them greedily. We prove convergence guarantees and show that ADMM-Q can serve as a drop-in replacement for standard layer-wise quantization solvers in PTQ pipelines that use equivalent transformations such as scaling and rotation. Empirically, ADMM-Q substantially improves perplexity and zero-shot accuracy across a broad range of model sizes, from Qwen 1.7B–32B in the weight-only setting and from 1B–8B in our SpinQuant experiments on Qwen and LLaMA, with especially pronounced gains at more aggressive quantization levels.

Limitations. Although ADMM-Q consistently improves quantized model quality, it introduces additional offline quantization cost relative to lightweight baselines such as RTN and GPTQ because it solves an iterative optimization problem for each layer. Similar to other PTQ approaches, ADMM-Q method relies on calibration activations and a Hessian approximation derived from them, so its performance may depend on how representative the calibration set is for the downstream task. Moreover, we evaluate ADMM-Q only on dense autoregressive decoder-only LLMs, not on mixture-of-experts architectures, diffusion language models, or vision transformers. Although the optimization framework is general, these settings have different structure and may require nontrivial adaptation.

References

- Josh Achiam, Steven Adler, Sandhini Agarwal, Lama Ahmad, Ilge Akkaya, Florencia Leoni Aleman, Diogo Almeida, Janko Altenschmidt, Sam Altman, Shyamal Anadkat, et al. Gpt-4 technical report. *arXiv preprint arXiv:2303.08774*, 2023.
- Saleh Ashkboos, Amirkeivan Mohtashami, Maximilian L Croci, Bo Li, Martin Cameroni, Torsten Hoeffler, James Hensman, and Dan Alistarh. QuaRot: Outlier-free 4-bit inference in rotated LLMs. In *Advances in Neural Information Processing Systems*, 2024.
- Pratyay Banerjee, Kuntal Kumar Pal, Arindam Mitra, and Chitta Baral. Careful selection of knowledge to solve open book question answering. *arXiv preprint arXiv:1907.10738*, 2019.
- Yonatan Bisk, Rowan Zellers, Jianfeng Gao, Yejin Choi, et al. Piqa: Reasoning about physical commonsense in natural language. In *Proceedings of the AAAI conference on artificial intelligence*, volume 34, pages 7432–7439, 2020.
- Stephen Boyd, Neal Parikh, Eric Chu, Borja Peleato, Jonathan Eckstein, et al. Distributed optimization and statistical learning via the alternating direction method of multipliers. *Foundations and Trends® in Machine learning*, 3(1):1–122, 2011.
- Vladimír Boža. Fast and optimal weight update for pruned large language models. *arXiv preprint arXiv:2401.02938*, 2024.
- Christopher Clark, Kenton Lee, Ming-Wei Chang, Tom Kwiatkowski, Michael Collins, and Kristina Toutanova. BoolQ: Exploring the surprising difficulty of natural yes/no questions. In Jill Burstein, Christy Doran, and Thamar Solorio, editors, *Proceedings of the 2019 Conference of the North American Chapter of the Association for Computational Linguistics: Human Language Technologies, Volume 1 (Long and Short Papers)*, pages 2924–2936, Minneapolis, Minnesota, June 2019. Association for Computational Linguistics. doi: 10.18653/v1/N19-1300. URL <https://aclanthology.org/N19-1300/>.
- Peter Clark, Isaac Cowhey, Oren Etzioni, Tushar Khot, Ashish Sabharwal, Carissa Schoenick, and Oyvind Tafjord. Think you have solved question answering? try arc, the ai2 reasoning challenge. *arXiv preprint arXiv:1803.05457*, 2018.
- Damek Davis and Wotao Yin. Convergence rate analysis of several splitting schemes. *Splitting methods in communication, imaging, science, and engineering*, pages 115–163, 2016.
- Tim Dettmers, Ruslan Svirschevski, Vage Egiazarian, Denis Kuznedelev, Elias Frantar, Saleh Ashkboos, Alexander Borzunov, Torsten Hoeffler, and Dan Alistarh. Spqr: A sparse-quantized representation for near-lossless llm weight compression. *arXiv preprint arXiv:2306.03078*, 2023.
- Abhimanyu Dubey, Abhinav Jauhri, Abhinav Pandey, Abhishek Kadian, Ahmad Al-Dahle, Aiesha Letman, Akhil Mathur, Alan Schelten, Amy Yang, Angela Fan, et al. The llama 3 herd of models. *arXiv preprint arXiv:2407.21783*, 2024.
- Elias Frantar and Dan Alistarh. Optimal brain compression: A framework for accurate post-training quantization and pruning. *Advances in Neural Information Processing Systems*, 35:4475–4488, 2022.
- Elias Frantar and Dan Alistarh. Sparsegpt: Massive language models can be accurately pruned in one-shot. In *International Conference on Machine Learning*, pages 10323–10337. PMLR, 2023.
- Elias Frantar, Saleh Ashkboos, Torsten Hoeffler, and Dan Alistarh. Gptq: Accurate post-training quantization for generative pre-trained transformers. *arXiv preprint arXiv:2210.17323*, 2022.
- L Gao, J Tow, B Abbasi, S Biderman, S Black, A DiPofi, C Foster, L Golding, J Hsu, A Le Noac’h, et al. A framework for few-shot language model evaluation. *Zenodo*, 2023. doi: 10.5281/zenodo.10256836.

- Gemini Team Google. Gemini: a family of highly capable multimodal models. *arXiv preprint arXiv:2312.11805*, 2023.
- Song Han, Huizi Mao, and William J Dally. Deep compression: Compressing deep neural networks with pruning, trained quantization and huffman coding. *arXiv preprint arXiv:1510.00149*, 2015.
- Babak Hassibi and David Stork. Second order derivatives for network pruning: Optimal brain surgeon. *Advances in neural information processing systems*, 5, 1992.
- Ji Lin, Jiaming Tang, Haotian Tang, Shang Yang, Wei-Ming Chen, Wei-Chen Wang, Guangxuan Xiao, Xingyu Dang, Chuang Gan, and Song Han. Awq: Activation-aware weight quantization for on-device llm compression and acceleration. *Proceedings of Machine Learning and Systems*, 6:87–100, 2024.
- Zechun Liu, Changsheng Zhao, Igor Fedorov, Bilge Soran, Dhruv Choudhary, Raghuraman Sridhar, Hyemin Kwon, Ivan Lazarevich, Vikas Bannur, Sachin Babu, et al. SpinQuant: LLM quantization with learned rotations. In *International Conference on Learning Representations*, 2025.
- Mehdi Makni, Xiang Meng, and Rahul Mazumder. 3BASil: An algorithmic framework for sparse plus low-rank compression of LLMs. In *The Thirty-ninth Annual Conference on Neural Information Processing Systems*, 2025. URL <https://openreview.net/forum?id=byMNv5Et10>.
- Xiang Meng, Kayhan Behdin, Haoyue Wang, and Rahul Mazumder. Alps: Improved optimization for highly sparse one-shot pruning for large language models. In *Annual Conference on Neural Information Processing Systems, NeurIPS*, 2024.
- Adam Paszke, Sam Gross, Soumith Chintala, Gregory Chanan, Edward Yang, Zachary DeVito, Zeming Lin, Alban Desmaison, Luca Antiga, and Adam Lerer. Automatic differentiation in pytorch. *NIPS Autodiff Workshop*, 2017.
- Adam Poliak. A survey on recognizing textual entailment as an nlp evaluation. *arXiv preprint arXiv:2010.03061*, 2020.
- Bernardino Romera-Paredes, Mohammadamin Barekatin, Alexander Novikov, Matej Balog, M. Pawan Kumar, Emilien Dupont, Francisco J. R. Ruiz, Jordan S. Ellenberg, Pengming Wang, Omar Fawzi, Pushmeet Kohli, and Alhussein Fawzi. Mathematical discoveries from program search with large language models. *Nat.*, 625(7995):468–475, January 2024. URL <https://doi.org/10.1038/s41586-023-06924-6>.
- Baptiste Roziere, Jonas Gehring, Fabian Gloeckle, Sten Sootla, Itai Gat, Xiaoqing Ellen Tan, Yossi Adi, Jingyu Liu, Romain Sauvestre, Tal Remez, et al. Code llama: Open foundation models for code. *arXiv preprint arXiv:2308.12950*, 2023.
- Keisuke Sakaguchi, Ronan Le Bras, Chandra Bhagavatula, and Yejin Choi. Winogrande: An adversarial winograd schema challenge at scale. *Communications of the ACM*, 64(9):99–106, 2021.
- Maarten Sap, Hannah Rashkin, Derek Chen, Ronan LeBras, and Yejin Choi. Socialliqa: Commonsense reasoning about social interactions, 2019. URL <https://arxiv.org/abs/1904.09728>.
- Mingjie Sun, Zhuang Liu, Anna Bair, and J. Zico Kolter. A simple and effective pruning approach for large language models, 2024. URL <https://arxiv.org/abs/2306.11695>.
- Guangxuan Xiao, Ji Lin, Mickael Seznec, Hao Wu, Julien Demouth, and Song Han. SmoothQuant: Accurate and efficient post-training quantization for large language models. In *International Conference on Machine Learning*, 2023.
- Fengli Xu, Qianyu Hao, Zefang Zong, Jingwei Wang, Yunke Zhang, Jingyi Wang, Xiaochong Lan, Jiahui Gong, Tianjian Ouyang, Fanjin Meng, et al. Towards large reasoning models: A survey of reinforced reasoning with large language models. *arXiv preprint arXiv:2501.09686*, 2025.

Rowan Zellers, Ari Holtzman, Yonatan Bisk, Ali Farhadi, and Yejin Choi. HellaSwag: Can a machine really finish your sentence? In Anna Korhonen, David Traum, and Lluís Màrquez, editors, *Proceedings of the 57th Annual Meeting of the Association for Computational Linguistics*, pages 4791–4800, Florence, Italy, July 2019. Association for Computational Linguistics. doi: 10.18653/v1/P19-1472. URL <https://aclanthology.org/P19-1472/>.

Appendix

A Integration of ADMM-Q with equivalent transformations

We spell out in more detail how equivalent transformations modify the local reconstruction problem solved by ADMM-Q. In each case, the transformation rewrites the layer in an equivalent form, after which ADMM-Q is applied to the transformed weight variable.

Scaling. Suppose a per-channel scaling matrix \mathbf{S} is applied before quantization. Then the layer can be rewritten as:

$$\mathbf{Y} = \mathbf{X}\mathbf{W} = (\mathbf{X}\mathbf{S}^{-1})(\mathbf{S}\mathbf{W}).$$

Define the scaled weight:

$$\mathbf{U} = \mathbf{S}\mathbf{W}, \quad \widehat{\mathbf{U}} = \mathbf{S}\widehat{\mathbf{W}}.$$

Then ADMM-Q is applied to the transformed local reconstruction problem

$$\min_{\mathbf{U}} \frac{1}{2} \text{Tr} \left((\mathbf{U} - \widehat{\mathbf{U}})^\top \mathbf{H}_{\text{sc}} (\mathbf{U} - \widehat{\mathbf{U}}) \right) \quad \text{s.t.} \quad \mathbf{U} \in \mathcal{Q}$$

where $\mathbf{H}_{\text{sc}} = \mathbf{X}_{\text{sc}}^\top \mathbf{X}_{\text{sc}} = (\mathbf{X}\mathbf{S}^{-1})^\top (\mathbf{X}\mathbf{S}^{-1}) = (\mathbf{S}^{-1})^\top \mathbf{H}\mathbf{S}^{-1}$. Similar to [Xiao et al. \(2023\)](#), we directly store the scaled quantized weights.

Rotation. Suppose rotation matrices $\mathbf{R}_1, \mathbf{R}_2$ are applied before quantization. Then the layer can be rewritten as:

$$\mathbf{Y} = \mathbf{X}\mathbf{W} = (\mathbf{X}\mathbf{R}_1)(\mathbf{R}_1^{-1}\mathbf{W}\mathbf{R}_2)\mathbf{R}_2^{-1}$$

Define the rotated weight:

$$\mathbf{U} = \mathbf{R}_1^{-1}\mathbf{W}\mathbf{R}_2, \quad \widehat{\mathbf{U}} = \mathbf{R}_1^{-1}\widehat{\mathbf{W}}\mathbf{R}_2$$

Then ADMM-Q is applied to the transformed local reconstruction problem:

$$\min_{\mathbf{U}} \frac{1}{2} \text{Tr} \left((\mathbf{U} - \widehat{\mathbf{U}})^\top \mathbf{H}_{\text{rot}} (\mathbf{U} - \widehat{\mathbf{U}}) \right) \quad \text{s.t.} \quad \mathbf{U} \in \mathcal{Q}$$

where $\mathbf{H}_{\text{rot}} = \mathbf{X}_{\text{rot}}^\top \mathbf{X}_{\text{rot}} = (\mathbf{X}\mathbf{R}_1)^\top (\mathbf{X}\mathbf{R}_1) = \mathbf{R}_1^\top \mathbf{H}\mathbf{R}_1$. As in other work ([Liu et al., 2025](#)), we directly store the rotated quantized weights.

B Additional Details on Grid Refresh

Here we give more detail on the grid-refresh step used in ADMM-Q. The main point is that the quantization grid is not part of the ADMM state in the same way as \mathbf{W} , \mathbf{D} , and \mathbf{V} ; rather, it determines how the projection in the \mathbf{D} -update is carried out. If the grid is chosen once at initialization and then held fixed, it can become misaligned with the continuous trajectory produced by ADMM.

Stale fixed grid. Let $\theta = (\Delta, z_0)$ denote the scale and zero-point that determine the quantization grid $\mathcal{Q}(\theta)$. At iteration t , the point projected in the \mathbf{D} -update is

$$\widetilde{\mathbf{W}}^{(t)} = \mathbf{W}^{(t+1)} + \mathbf{V}^{(t)} / \rho_t.$$

With a fixed grid θ , the discrete update is

$$\mathbf{D}^{(t+1)} = \Sigma^{-1} \text{Proj}_{\mathcal{Q}(\theta)}(\Sigma \widetilde{\mathbf{W}}^{(t)}).$$

In practice, θ is typically initialized by RTN to the dense weights. Early in the ADMM iterations this is a reasonable choice, but as the continuous iterates move, the projection induced by that initial grid may no longer be well matched to the current $\widetilde{\mathbf{W}}^{(t)}$. The projected point can therefore be unnecessarily far from the current continuous ADMM target.

Refreshed grid. To address this, we equip ADMM-Q with the ability to recompute the grid parameters from the current continuous weights using the same scale/zero-point fitting routine used at initialization. This gives refreshed parameters $\theta_{\text{new}} = (\Delta_{\text{new}}, z_{0,\text{new}})$, and the same target $\widetilde{\mathbf{W}}^{(t)}$ is then re-projected onto the refreshed grid:

$$\mathbf{D}_{\text{new}}^{(t+1)} = \Sigma^{-1} \text{Proj}_{\mathcal{Q}(\theta_{\text{new}})}(\Sigma \widetilde{\mathbf{W}}^{(t)}).$$

The role of the refresh is therefore not to change the continuous ADMM iterate itself, but to update the projection map so that the discrete point better matches the current continuous trajectory.

Acceptance and dual consistency. We accept a refreshed grid only when the updated quantized weights improves \mathbf{D} -update objective. If the current projected point is $\mathbf{D}_{\text{old}}^{(t+1)}$ and the refreshed projection is $\mathbf{D}_{\text{new}}^{(t+1)}$, the acceptance criteria reads:

$$\left\| \mathbf{D}_{\text{new}}^{(t+1)} - \left(\mathbf{W}^{(t+1)} + \mathbf{V}^{(t)} / \rho_t \right) \right\|_F^2 \leq \left\| \mathbf{D}_{\text{old}}^{(t+1)} - \left(\mathbf{W}^{(t+1)} + \mathbf{V}^{(t)} / \rho_t \right) \right\|_F^2. \quad (13)$$

After accepting the refresh we replace the discrete point by $\mathbf{D}_{\text{new}}^{(t+1)}$ and update the dual variable as:

$$\mathbf{V} \leftarrow \mathbf{V} + \rho_t (\mathbf{D}_{\text{old}}^{(t+1)} - \mathbf{D}_{\text{new}}^{(t+1)}). \quad (14)$$

This preserves consistency of the current ADMM state after the discrete projection has been changed. To avoid repeated interventions in the projection map from affecting the convergence behavior of the base ADMM iterations, we allow at most one accepted grid refresh.

C Proof of Theorem 1

We first build a key inequality:

$$\left\| \mathbf{D}^{(t+1)} - \left(\mathbf{W}^{(t+1)} + \mathbf{V}^{(t)} / \rho_t \right) \right\|_F^2 \leq \left\| \mathbf{D}^{(t)} - \left(\mathbf{W}^{(t+1)} + \mathbf{V}^{(t)} / \rho_t \right) \right\|_F^2. \quad (15)$$

Proof. We consider two scenarios.

Case 1: The quantization grid is fixed during this iteration. Since the update rule (10) rounds each element of $\mathbf{W}^{(t+1)} + \mathbf{V}^{(t)} / \rho_t$ to its nearest point on the quantization grid, it turns out that \mathbf{D}^{t+1} satisfies

$$\mathbf{D}^{(t+1)} = \arg \min_{\Sigma \mathbf{D} \in \mathcal{Q}} \left\| \mathbf{D} - \left(\mathbf{W}^{(t+1)} + \mathbf{V}^{(t)} / \rho_t \right) \right\|_F^2. \quad (16)$$

Therefore, for any \mathbf{D} such that $\Sigma \mathbf{D} \in \mathcal{Q}$, it holds

$$\left\| \mathbf{D}^{(t+1)} - \left(\mathbf{W}^{(t+1)} + \mathbf{V}^{(t)} / \rho_t \right) \right\|_F^2 \leq \left\| \mathbf{D} - \left(\mathbf{W}^{(t+1)} + \mathbf{V}^{(t)} / \rho_t \right) \right\|_F^2. \quad (17)$$

Since $\Sigma \mathbf{D}^{(t)} \in \mathcal{Q}$, inequality (15) holds.

Case 2: The quantization grid has been updated during this iteration. According to the algorithm, we can simplify the update rule as: performing \mathbf{W} -update as usual; find $\mathbf{D}_{\text{new}}^{(t+1)}$ on the new quantization grid; and

finally the \mathbf{V} -update $\mathbf{V}^{(t+1)} = \mathbf{V}^{(t)} + \rho_t(\mathbf{W}^{(t+1)} - \mathbf{D}_{\text{new}}^{(t+1)})$. Note that we will only refresh the grid only if it improves \mathbf{D} -update objective. Together with the discussion in Case 1, it follows that

$$\begin{aligned} \left\| \mathbf{D}_{\text{new}}^{(t+1)} - \left(\mathbf{W}^{(t+1)} + \mathbf{V}^{(t)} / \rho_t \right) \right\|_F^2 &\leq \left\| \mathbf{D}_{\text{old}}^{(t+1)} - \left(\mathbf{W}^{(t+1)} + \mathbf{V}^{(t)} / \rho_t \right) \right\|_F^2 \\ &\leq \left\| \mathbf{D}^{(t)} - \left(\mathbf{W}^{(t+1)} + \mathbf{V}^{(t)} / \rho_t \right) \right\|_F^2. \end{aligned} \tag{18}$$

□

The rest of convergence proof builds primarily on the analysis of (Meng et al., 2024, Theorem 1), since the update rules for \mathbf{W} and \mathbf{V} remain unchanged. The convergence argument in (Meng et al., 2024, Theorem 1) transfers to our setting without modification. We conclude that both $\{\mathbf{D}^{(t)}\}_{t=0}^{\infty}$ and $\{\mathbf{W}^{(t)}\}_{t=0}^{\infty}$ converge to a shared limit $\bar{\mathbf{D}}$, which completes the proof.

D Additional Experimental Details

Computing environments. All experiments were conducted on a computing cluster. Unless otherwise specified, we utilized an Intel Xeon Gold 6248 machine with 16 CPU cores and a single NVIDIA L40 48GB / A100 80GB / H100 80GB GPU/ H200 144GB GPU. When runtime compression results are reported, all experiments have been run on the same node (including GPU) configuration. All language models and quantization methods were implemented using the PyTorch library (Paszke et al., 2017).

Implementation details of ADMM-Q. Following Frantar et al. (2022), we add a damping term to the Hessian: $\mathbf{H}' = \mathbf{H} + 0.01 \cdot \text{Tr}(\mathbf{X}^\top \mathbf{X})\mathbf{I}$.

We use $T = 300$ maximum number of ADMM iterations with initial penalty $\rho_0 = 0.1$ and $\gamma = 1.1$.

The MSE grid search for clipping ratios uses 100 grid points with maximum shrink ratio 0.8. For integration with SpinQuant, ADMM-Q replaces only the GPTQ weight quantization step; all rotation optimization, activation quantization, and KV cache quantization remain unchanged from the SpinQuant pipeline.

Algorithm Runtime and Memory Results. Table 5 reports wall-clock quantization time and peak GPU memory usage for GPTQ and ADMM-Q on Qwen3 weight-only quantization. While ADMM-Q consistently delivers better quantized model quality in our experiments, it does so by replacing GPTQ’s greedy one-pass updates with an iterative optimization procedure, so some additional offline cost is expected. The table shows that the runtime overhead grows with model size, but remains practically manageable: even for Qwen3-32B, quantization finishes in under two hours for both methods. Peak memory, reported as a ratio normalized so that ADMM-Q equals 1.0, shows that GPTQ uses roughly 94% of ADMM-Q’s peak across all model sizes, a consistent but modest difference. Since weight quantization is a one-time preprocessing step rather than part of inference-time deployment, we view both the increase in runtime and the slightly higher peak memory as reasonable tradeoffs for the consistent gains in perplexity and zero-shot accuracy.

Model	Runtime (min)		Peak quant. memory		Peak inference memory			Storage memory		
	GPTQ	ADMM-Q	GPTQ	ADMM-Q	Dense	GPTQ	ADMM-Q	Dense	GPTQ	ADMM-Q
1.7B-Base	1.95	2.22	0.956 ± 0.012	1.000	1.000	0.285 ± 0.013	0.294 ± 0.024	1.000	0.255	0.255
4B-Base	4.44	7.20	0.943 ± 0.014	1.000	1.000	0.281 ± 0.015	0.285 ± 0.018	1.000	0.254	0.255
8B-Base	7.31	13.91	0.938 ± 0.013	1.000	1.000	0.279 ± 0.017	0.282 ± 0.012	1.000	0.253	0.254
14B-Base	13.27	33.79	0.944 ± 0.012	1.000	1.000	0.284 ± 0.011	0.284 ± 0.012	1.000	0.253	0.253
32B	33.97	117.73	0.941 ± 0.013	1.000	1.000	0.273 ± 0.010	0.273 ± 0.008	1.000	0.252	0.253

Table 5: Wall-clock quantization time (minutes) and memory usage metrics. Peak quantization memory compares GPTQ and ADMM-Q, normalized so ADMM-Q is 1; values below 1 indicate lower peak memory usage than ADMM-Q. Peak inference memory and storage memory, with Dense normalized to 1, indicate that both GPTQ and ADMM-Q use approximately 28% of the memory during inference and take up just over 25% as much storage memory.

Ablation Study on ADMM-Q Algorithm Components. Table 6 shows that the performance gains of ADMM-Q come from the combination of its main components. At W4, the full method improves over GPTQ on all three perplexity metrics, reducing Wiki-2 from 7.82 to 7.56, C4 from 13.39 to 13.01, and PTB from 19.82 to 19.04, while remaining competitive in zero-shot accuracy. At W3, the same pattern is more pronounced: ADMM-Q substantially improves over GPTQ, reducing Wiki-2 from 12.85 to 10.06, C4 from 21.27 to 18.25, and PTB from 35.01 to 27.30, while also improving zero-shot accuracy from 54.43 to 57.80. Among the individual ablations, removing diagonal preconditioning causes the largest loss, especially at 3 bits, indicating that conditioning the layer-wise subproblem is critical for effective ADMM updates. Removing adaptive ρ also leads to a clear drop in quality, while local search provides a smaller but still meaningful gain overall. When all three components are disabled, performance deteriorates sharply, particularly at W3.

Method	W4				W3			
	Wiki-2	C4	PTB	0-shot	Wiki-2	C4	PTB	0-shot
Dense	7.00	11.91	17.12	69.07	7.00	11.91	17.12	69.07
GPTQ	7.82	13.39	19.82	68.93	12.85	21.27	35.01	54.43
ADMM-Q (full)	7.56	13.01	19.04	68.14	10.06	18.25	27.30	57.80
w/o local search	7.58	13.11	19.22	68.41	9.93	18.44	28.95	57.36
w/o adaptive ρ	7.73	13.24	19.46	67.63	10.97	19.86	30.81	55.23
w/o diag. precondition.	8.03	13.66	20.59	66.95	14.68	26.42	45.74	50.83
all off	9.64	16.34	26.52	65.79	42.47	57.76	115.86	41.94

Table 6: Ablation study for ADMM-Q on Qwen3-8B-Base under symmetric per-channel weight-only quantization at 4 bits (W4) and 3 bits (W3). PPL columns (\downarrow) report perplexity on WikiText-2, C4, and Penn Treebank; 0-shot (\uparrow) is average zero-shot accuracy. Dense and GPTQ are shown for reference. The same qualitative pattern holds at both precisions, but the impact of removing key components is substantially larger at 3 bits, particularly for diagonal preconditioning.

Ablation Study on ADMM-Q with SpinQuant. Table 7 extends the ablation study to the weight-and-activation setting (WbA4KV4) with SpinQuant on LLaMA-3 8B and LLaMA-3.2 1B-Instruct. In this more constrained setting, local search and adaptive ρ are the most impactful components, each causing substantial degradation when removed, particularly at W3 where removing either one roughly doubles the perplexity gap to the dense baseline on LLaMA-3 8B. Diagonal preconditioning provides a smaller but steady improvement across all configurations. The “all off” configuration degrades catastrophically at W3, reaching perplexities above 150 on the smaller model, confirming that all three components are essential for stable low-bit quantization in the weight-and-activation setting.

Method	LLaMA-3 8B — W4A4KV4				LLaMA-3 8B — W3A4KV4				1B-Inst. — W4A4KV4				1B-Inst. — W3A4KV4			
	Wiki-2	C4	PTB	0-shot	Wiki-2	C4	PTB	0-shot	Wiki-2	C4	PTB	0-shot	Wiki-2	C4	PTB	0-shot
Dense	6.14	9.44	14.84	63.94	6.14	9.44	14.84	63.94	13.16	21.30	37.31	53.22	13.16	21.30	37.31	53.22
GPTQ	7.34	12.16	17.94	60.55	8.50	15.01	21.27	56.51	15.81	26.11	48.69	48.27	19.70	34.07	65.22	45.76
ADMM-Q (full)	7.26	12.08	17.74	60.52	8.02	14.29	20.13	57.59	15.55	25.80	47.76	49.31	17.88	31.16	56.65	46.84
w/o local search	7.97	13.09	18.93	58.32	10.93	20.91	29.32	51.06	19.45	31.18	58.28	46.20	28.12	48.41	100.83	42.74
w/o adaptive ρ	7.94	13.16	19.17	57.96	11.52	22.00	31.97	51.78	17.45	28.28	53.96	48.39	28.32	49.34	91.35	42.85
w/o diag. precondition.	7.65	12.72	18.59	58.43	9.44	17.39	25.30	54.44	16.03	26.52	48.72	48.79	19.76	35.48	66.57	45.17
all off	8.89	14.43	20.98	57.12	56.35	82.98	174.21	40.46	21.87	33.58	65.31	45.71	150.16	184.86	396.32	37.80

Table 7: Ablation study for ADMM-Q within the SpinQuant pipeline on LLaMA-3 8B and LLaMA-3.2 1B-Instruct under symmetric per-channel W4A4KV4 quantization at 4 bits (W4) and 3 bits (W3). PPL columns (\downarrow) report perplexity on WikiText-2, C4, and Penn Treebank; 0-shot (\uparrow) is average zero-shot accuracy. Dense and GPTQ baselines are shown for reference.